Title
Front Cover: Effects of Microstructural Properties on Auxeticity and Negative Thermal Expansion of a Class of 2D Lattice Systems (Phys. Status Solidi B 7/2026)

Journal
physica status solidi (b), 263(7)

ISSN
0370-1972

Authors
Wang, Yun-Che
Lee, Chia-Ju
Liao, Tse-Chun
et al.

Publication Date
2026-07-01

DOI
10.1002/pssb.70287

Peer reviewed

Effects of microstructural properties on auxeticity and negative thermal expansion of a class of 2D lattice systems

Yun-Che Wang[1,*], Chia-Ju Lee[1], Tse-Chun Liao[1], Yasothorn Sapsathiarn[2], Jiun-Shyan Chen[3]

[1]Department of Civil Engineering, National Cheng Kung University, Tainan, Taiwan

[2]Department of Civil and Environmental Engineering, Mahidol University, Nakorn Pathom, Thailand

[3]Department of Structural Engineering, University of California San Diego, La Jolla, CA, USA

*Corresponding author: yunche@ncku.edu.tw

Abstract

We study auxetic lattice structures with curved bi-material ligaments using the finite element method. The overall Poisson's ratio and coefficient of thermal expansion of the lattices can be simultaneously tuned to be negative by adjusting their microstructural geometries and constituent material parameters. The Young's modulus of ligaments plays an important role in controlling the effective Poisson's ratio and coefficient of thermal expansion. The size and Young's modulus of the joints that connect ligaments strongly affect the effective mechanical properties. When Young's modulus of the joint is given, a larger joint size gives rise to stronger auxeticity, but less negative thermal expansion. By tuning the coefficient of thermal expansion of each constituent, the overall coefficient of thermal expansion may be negative, zero or positive. The bicamaterial auxetic structures studied here may be designed to possess desired properties for real-world applications when their microstructural properties are appropriately tuned.

Introduction

Mechanical metamaterials and composite materials have been under intensive study in recent years for their unique and unusual properties [1,2,3]. One of the unusual properties is the negative Poisson's ratio (NPR) [4,5,6,7]. The Poisson's ratio is defined by the ratio of lateral strain to the longitudinal strain with a minus sign as $\nu = -\varepsilon_{yy}/\varepsilon_{xx}$, when the prismatic material is under the longitudinal straining ε_{xx}. Various mechanisms have been proposed to generate auxeticity, such as the connected stars as auxetic systems [8,9]. The terms "auxeticity" and "negative Poisson's ratio" are used interchangeably. Giant NPR from patterned slit perforations within a sheet/block of material has been reported [10]. Ref. [11] has studied NPR in lattice structures with sinusoidal ligaments. The deformation mechanism of NPR due to the re-entrant cell shapes has been discussed in detail [12]. The re-entrant shape is also called inverted hexagons, as opposed to the regular hexagons in the honeycomb structures [13]. In addition, effects of inhomogeneity in gradient auxetic closed cell foams on NPR have been analyzed and experimentally studied [14]. Furthermore, the tunability of NPR can be achieved in certain novel microstructures [15,16]. Negative Poisson's ratio at the molecular level has been investigated [17,18], including the α-cristobalite tetrahedral framework [19,20], and crystalline cellulose I_{β} [21]. Recently, molecular systems containing nanochannels and nanolayers as a second phase have been shown to exhibit NPR [22,23]. Moreover, the ordering of the second phase can be used as a fine-tuning parameter to change the Poisson's ratio of the molecular systems.

Regardless of microstructures, the theory of elasticity states that, in order to satisfy the pointwise stability condition that strain energy is positive definite [24], the Poisson's ratio of isotropic three-dimensional materials is in the range between -1 and 0.5. For two-dimensional materials, their Poisson's ratio is between – 1 and 1 [25,26,27,28,29]. The cross-sectional shape of ligament in cubic lattices can be used as a strategy to tune the effective Poisson's ratio to be positive or negative [30]. The characteristic of the anticlastic curvature in negative Poisson's ratio materials has recently been further studied [31]. In addition, chirality arising from non-centrosymmetry may also give rise to auxeticity [32,33,34]. Recently, the valid range of Poisson's ratio in chiral solids has been extended beyond classical limits [35,36]. Chirality can also affect the bandgap structures in the negative Poisson's ratio materials [37]. Furthermore, chiral effects on viscoelastic properties have been reported [38].

A related research area is the use of negative stiffness to obtain unbounded overall properties in composite materials [39,40,41,42,43,44]. Unlike auxeticity, the stability of negative stiffness systems for extreme effective properties requires careful considerations [45,46,47,48,49]. Simultaneously achieving negative stiffness and negative Poisson's ratio has been experimentally demonstrated and analyzed [50].

In addition to negative Poisson's ratio, metamaterials have also been widely studied for their negative thermal expansion (NTE) in the bi-material lattices [51,52,53], albeit NTE in two-phase composite materials has been studied quite some time ago [54]. Microstructured isotropic media that are mechanically auxetic and thermally shrink under heating have been investigated [55]. Metamaterials with the unimodal deformation mechanism for negative thermal expansion and compressibility have been investigated [56,57,58]. In addition, rotating-square microstructures for negative thermal expansion have been analyzed [59]. Furthermore, tunable positive to negative thermal expansion in metamaterials has been reported [60,61,62,63,64], as well as in Ref. [65] for tunable hygrothermal expansion. Negative thermal expansion has also been studied at the molecular levels [66,67,68]. Recently, simultaneously obtaining a negative Poisson's ratio and a negative thermal expansion has been reported for the curvature effects in the bi-material lattice [69,70]. In this work, we provide a further detailed analysis of the systems on the effects of microstructural properties, including the joint size and its elasticity. In the literature, two-dimensional auxetic foams with Y-joint and Δ-joint geometry have been investigated [71].

In this work, we conduct the finite element analysis [72] to study the negative Poisson's ratio and thermal expansion of a class of 2D and 3D auxetic structures with COMSOL software [73]. Effects of the material properties of the two constituents in the bi-material ligaments on the overall thermoelastic properties of the lattices are investigated, as well as the effects of the joint size and its Young's modulus.

Estimation of effective properties

The effective thermoelastic properties of composite materials comprising fully anisotropic phases can be estimated from constituents' properties in the Hashin-Shtrikman sense by the following two equations [74].

$$\mathbf{C}_e = \mathbf{C}_m[\mathbf{I} + f\,\mathbf{JK}(\mathbf{C}_m - \mathbf{C}_i)]^{-1} \tag{1}$$

$$\boldsymbol{\alpha}_e = \boldsymbol{\alpha}_m + f\,\mathbf{JKC}_i(\boldsymbol{\alpha}_i - \boldsymbol{\alpha}_m) \tag{2}$$

Here $\mathbf{C}_e$ is the 6 x 6 matrix of the effective elastic constants, and $\boldsymbol{\alpha}_e$ the 6 x 1 vector of the effective coefficient of thermal expansion (CTE). The subscripts m and i indicate the matrix and inclusion, respectively. The inclusion volume fraction is denoted by *f*. The matrices **J** and **K** are defined in terms of the Eshelby matrix **S** as follows.

$$\mathbf{J} = [\mathbf{I} - f\,\mathbf{K}(\mathbf{C}_m - \mathbf{C}_i)(\mathbf{I} - \mathbf{S})]^{-1} \tag{3}$$

$$\mathbf{K} = [\mathbf{C}_m - (\mathbf{C}_m - \mathbf{C}_i)\mathbf{S}]^{-1} \tag{4}$$

The above equations can be algebraically recast into the following equation with the Eshelby matrix for the effective coefficient of thermal expansion.

$$\boldsymbol{\alpha}_e = \boldsymbol{\alpha}_m + \left(\mathbf{C}_c^{-1} - \mathbf{C}_m^{-1}\right)\mathbf{C}_m\left(\mathbf{C}_m - \mathbf{C}_i\right)^{-1}(\boldsymbol{\alpha}_i - \boldsymbol{\alpha}_m) \tag{5}$$

By switching the roles of matrix and inclusion, an upper and lower bound on the effective thermoelastic properties can be obtained from the above equations. Furthermore, these equations can be reduced for the isotropic constituents [75,76]. When the microstructures are known, as in this study, the effective thermoelastic properties can be calculated from the averaged stress and strain tensors, defined as follows [41], via the finite element analysis.

$$\bar{\sigma}_{ij} = \frac{1}{V}\int_V \sigma_{ij} dV = \frac{1}{V}\int_A t_i x_j dA \tag{6}$$

$$\bar{\varepsilon}_{ij} = \frac{1}{V}\int_V \varepsilon_{ij} dV = \frac{1}{2V}\int_A (u_i n_j + u_j n_i) dA \tag{7}$$

The volume integrals require all the stress and strain information in the domain, while the area integrals only require the information on the boundary surfaces. With the averaged stress and strain tensor, the effective Young's modulus E_e, two-dimensional bulk modulus B_e and biaxial shear modulus G_{be} can be calculated by

$$E_e = \frac{\bar{\sigma}_{11}}{\bar{\varepsilon}_{11}} \tag{8}$$

$$B_e = \frac{\bar{\sigma}_{11} + \bar{\sigma}_{22}}{2(\bar{\varepsilon}_{11} + \bar{\varepsilon}_{22})} \tag{9}$$

$$G_{be} = \frac{\bar{\sigma}_{22}}{2\bar{\varepsilon}_{22}} \tag{10}$$

The biaxial shear loading condition is defined when ¯ = ¯ , where ¯ is the averaged stress on the left and right edge of the specimen, and ¯ is the averaged stress on the top and bottom edge. In addition, the effective Poisson's ratio can be calculated by

$$\nu_e = -\frac{\bar{\varepsilon}_{22}}{\bar{\varepsilon}_{11}} \tag{11}$$

when the stress element is under x-direction straining ¯ , and the effective coefficient of thermal expansion by

$$\alpha_e = \frac{1}{2\Delta T}(\bar{\varepsilon}_{11} + \bar{\varepsilon}_{22}) \tag{12}$$

where ΔT is the uniform temperature change applied to the whole specimen.

Computational models and settings

Figures 1 (a), (c) and (e) show the two-dimensional auxetic structures and their unit cells around the joint are shown in Figures 1 (b), (d) and (f). The structures possess 2D cubic symmetry and are analyzed along their principal directions, i.e. the horizontal and vertical directions. The three structures, labeled as the “small”, “medium” and “large” structure, have the same radius of midline curvature R_c = 5 cm for each bi-material ligament, but have different square joint sizes. The edge lengths of the joint and unit cell of the “small” structure are L_j = 0.18 cm and L_{cell} = 6.58 cm, those of the “medium” structure L_j = 0.82 cm and L_{cell} = 7.22 cm, and those of the “large” structure L_j = 1.55 cm and L_{cell} = 7.95 cm. To facilitate data analysis and discussion, the joint size is normalized to cell size, i.e. $L_j^n = Lj/L_{cell}$, and hence they are L_j^n = 0.028, 0.114, 0.195 for the three structures. The corresponding area fractions of the small, medium and large structure are f = 0.165, 0.197 and 0.245, respectively. In our models, larger joint sizes result in larger area fractions. Although the systems are analyzed for their linear thermoelastic responses in this work, it is intended for future analysis of the effects of nonlinearity and damage on the overall auxetic and NTE properties by more involved numerical methods, such as the one discussed in Ref. [77].

Each bi-material ligament consists of two different isotropic, homogeneous materials, as shown in Figure 1. Orange color is for Material 1 with Young's modulus E_1 and Poisson’s ratio ν_1. The yellow color indicates Material 2, with Young's modulus E_2 and Poisson's ratio ν_2. The alternate arrangement of Material 1 and Material 2 is noted. The square joint having Young's modulus E_j and Poisson’s ratio ν_j is in cyan color, and the boundary rectangles in green color. The boundary rectangles are assigned a very large Young's modulus for the purpose of loading and deformation measurement.

In order to analyze the structures, the finite element method is adopted to numerically calculate their effective properties from effective stress by Eq. (6) and effective strain by Eq. (7). The number of triangular elements used in the small-, medium-, and large-joint-size models is 15196, 10256, and 8964, respectively. More elements are used when the joint size is smaller to obtain more accurate results in models with large stress and strain gradients. The shape function used in our finite element calculation was the fifth-order Lagrange polynomial function, i.e. six nodes on an edge of a triangular element. Full integration was used to evaluate the elastic and thermal fields in each element. Mesh sensitivity studies have been investigated, and our results reported here are consistent with data from denser meshes.

For the mechanical responses, such as effective Young’s modulus E_e and Poisson’s ratio ν_e, the displacement boundary condition of the left and bottom edges is set to be rollers, and uniform tensile straining is applied on the right edge. The upper edge is stress-free. Rollers allow sliding in one direction but constrain any rotation of the edges. For thermal responses, the structures are subjected to a uniform temperature change, and roller boundary conditions are applied at the left and bottom edges. We choose the boundary conditions so that our results can be directly compared with possible experimental prototypes. Due to the small number of cells in the models and no periodic boundary conditions employed in the 2D models, we acknowledge our results are influenced by the boundary conditions on the edges; hence, they may be model-size-dependent. When the system contains a large number of unit cells, the effects of boundary conditions may be neglected, and the calculated homogenized properties may be consistent with those obtained under periodic boundary conditions.

Results and discussion

To demonstrate the effects of the Young's modulus of ligament, the model shown in Figure 1 (c) is chosen. Figure 2 and Figure 3, respectively, show the effective Poisson's ratio and coefficient of thermal expansion of the three auxetic structures against the normalized Young's modulus of the bi-material ligament. As can be seen from the figures, simultaneous negative Poisson's ratio and negative CTE can be achieved. Figure 2 (b) is an enlarged version of Figure 2 (a) when E_1 is near E_2, and the sensitivities of the effective Poisson's ratio and CTE with respect to the logarithmic Young's modulus of ligament are identified in Figure 2 (b). The slopes of effective coefficient of thermal expansion with respect to the logarithmic Young's modulus of ligament are identified in Figure 3. When E_1 (or E_2) is under sweep, we set $E_0 = E_2$ (or $E_0 = E_1$) as the normalization parameter. Hence, when $E_1/E_0 = 1$ or $E_2/E_0 = 1$, it indicates $E_1 = E_2$, and the bi-material ligament is composed of a single material. In the calculation, E_0 is set to be 100 GPa, as the normalization Young's modulus.

Effects of joint size and normalized Young's modulus (E_j^n) of the joint on effective Poisson's ratio, Young's modulus, plane-strain bulk modulus, and biaxial shear modulus are shown in Figures 4, 5, 6 and 7, respectively. Figure 8 shows the effective coefficient of thermal expansion versus the joint's Young's modulus. When the Young's modulus of the joint is small, the dependence of the effective Poisson's ratio on the joint's Young's modulus is indicated in Figure 4. The slopes of the effective Poisson's ratio with respect to the logarithmic joint Young's modulus are m_S = -1.389, m_M = -3.311, and m_L = -3.769 for the small, medium and large models, respectively. The slope of the larger joint size model is more negative. When the joint's Young's modulus is large, no strong dependence between theall calculated effective properties and the joint's Young's modulus is observed. It is because when the joint's Young's modulus is large, the joint may behave as a relatively rigid unit in the structures. Hence, asymptotically plateau behavior is observed when E_j^n is large.

The effective Young's modulus of the three structures is shown in Figure 5. The slopes of the effective Young's modulus with respect to the logarithmic joint Young's modulus are m_S = 9.81, m_M = 16.00, m_L = 16.66. The medium and large joint models show similar slopes for overall

Young's modulus. However, the slope of the small joint model is less than that of the other two models.

For isotropic and homogeneous materials, the plane-strain bulk modulus, defined in Eq. (9), can be expressed as $B_e = \lambda+\mu = (C_{11}+C_{12})/2 = \mu(1+\nu)/(1-\nu)$, and bi-axial shear, defined in Eq. (10), can be expressed as $G_{be} = (C_{11}-C_{12})/2$. From Figure 6. When $E_j^n \sim 0.1$, the normalized effective 2D bulk modulus of the large model is about 20 x 10^{-3}, which is about the same as that of the small model. When $E_j^n \sim 2.3$, the normalized effective 2D bulk modulus is about 44 x 10^{-3} for both the medium and large model. From Figure 7, when $E_j^n \sim 0.22$, all three models show similar normalized effective shear modulus $G_{be} \sim 0.56$. However, the three curves do not coincide at a single point, but their intersecting points are very close. The crossovers among the curves can be used to design the auxetic structures to achieve certain purposes.

From Figure 8, the small model exhibits the strongest effective negative coefficient of thermal expansion, which is about -24 x 10^{-5} (1/K). All three models show similar trends when E_j^n increases. In Figure 9 (a), we set $E_j^n = 1$, and study the variations of α_1 and α_2 on the effective thermal expansion. When α_1 parameter is under scanning (red curves), the value of $\alpha_2 = 10^{-6}$ (1/K) is fixed. When the α_2 parameter varies (black curves), the value of $\alpha_1 = 10^{-4}$ (1/K) is fixed. With a given structure, the effective coefficient of thermal expansion can be tuned to be positive, zero or negative by choosing suitable α_1 or α_2, as can be seen in Figure 9 (b) in terms of the absolute value of the coefficient of thermal expansion. For the black curves, CTE is positive on the right hand side of the anti-peaks, and negative on their left hand side. For the red curves, CTE is negative on the right hand side of the anti-peaks, and positive on their left hand side. The anti-peaks indicate zero CTE. Zero thermal expansion coefficient is particularly intriguing for materials design, especially in avoiding residual stress under large temperature variations or thermal loadings. Furthermore, controlling the thermal expansion coefficient could allow for residual stress control in stability manipulation. The deformation of the small structure under uniform temperature change is shown in Figure 10 (a), as a demonstration. The von Mises stress around the small joint is shown in Figure 10 (b).

In this work, it is found that the geometric size and the elastic properties of the joints, in combination with ligament's thermoelastic properties affect the effective Poisson's ratio and thermal expansion. Large joints with sufficient elastic modulus may exhibit high rigidity, which may make the joints behave like a rigid rotating block in the microstructure, giving rise to more negative Poisson's ratio, as shown in Figure 4. However, for thermal expansion, smaller joints may yield more negative CTE, as the solid curves shown in Figures 8, 9 (a) and (b). Therefore, when in design for simultaneous NPR and negative CTE, the designer needs to pay attention to the subtle detail of microstructure.

We acknowledge that the overall properties studied here are only from the lattices with the 4x4 unit cells under the prescribed loading and boundary conditions. More unit cells in the lattices would reduce boundary effects. One may alternatively use periodic boundary conditions to reduce boundary effects. Our study here reveals quantitative relationships between constituents' properties and overall properties for the specifically chosen structures.

Conclusion

Through our finite element calculations, the effects of microstructural properties, including joint size and Young's modulus, on the overall properties of the 2D bi-material auxetic lattices are demonstrated in this work. Simultaneously achieving auxeticity and negative thermal expansion, or other combinations, has been quantitatively analyzed in our parametric study. Under a given joint Young's modulus, a larger joint size gives rise to stronger auxeticity, but less negative thermal expansion. The joint size affects the area fraction. The effective mechanical properties, such as effective Young's modulus, 2D bulk modulus, and biaxial shear modulus, increase with the E_j for a given L_j. By tuning the coefficient of thermal expansion of the constituent, the overall coefficient of thermal expansion may be negative, zero or positive. The bi-material auxetic structures studied in this work may be designed to possess desired properties through microstructural control for real-world applications.

Acknowledgements

This research is partially supported by the NSTC grant No. 112-2221-E-006-049-MY3, and Yushan Fellow Program (Project No. MOE-113-YSFEE-0005-001-P1) by the Ministry of Education (MOE), Taiwan.

References

1 R.S. Lakes, Materials that exceed classical thermodynamic bounds on properties, Reviews of Modern Physics 97, 021002 (2025)

2 R. Lakes, *Composites and Metamaterials*, World Scientific, Singapore, 2020.

3 T.C. Lim, Mechanics of Metamaterials with Negative Parameters, Springer, Springer Science and Business Media Singapore, 2020.

4 R. Lakes, Foam structures with a negative Poisson's ratio, Science 235, 1038-1040 (1987)

[5] R.S. Lakes, Negative-Poisson's-ratio materials: auxetic solids, Annual Review of Materials Research 47, 63-81 (2017)

[6] G. Milton, Composite materials with Poisson's ratios close to -1, Journal of the Mechanics and Physics of Solids 40, 1105-1137 (1992)

[7] T.C. Lim, Auxetic materials and structures, Springer Science and Business Media Singapore, 2015.

[8] J.N. Grima, R. Gatt, A. Alderson, K.E. Evans, On the potential of connected stars as auxetic systems, Molecular Simulation 31, 925-935 (2005)

[9] J.N. Grima, D. Attard, R. Caruana-Gauci, R. Gatt, Negative linear compressibility of hexagonal honeycombs and related systems, Scr. Mater 65, 565–568 (2011)

[10] L. Mizzi, K.M. Azzopardi, D. Attard, J.N. Grima, R. Gatt, Auxetic metamaterials exhibiting giant negative Poisson's ratios, Phys. Status Solidi RRL 9, 425-430 (2015)

[11] T. Strek, H. Jopek, K.W. Wojciechowski, The influence of large deformations on mechanical properties of sinusoidal ligament structures, Smart Materials and Structures 25, 054002 (2016)

[12] R. Lakes, Deformation mechanisms in negative Poisson's ratio materials: structural aspects, Journal of Materials Science 26, 2287-2292 (1991)

[13] L.J. Gibson, M.F. Ashby, G.S. Schajer, C.I. Robertson, The mechanics of two-dimensional cellular materials, Proceedings of the Royal Society A - Mathematical Physical and Engineering Sciences 382, 25-42 (1982)

[14] O. Duncan, A. Alderson, T. Allen, Fabrication, characterization and analytical modeling of gradient auxetic closed cell foams, Smart Mater. Struct. 30, 035014 (2021)

[15] T.-C. Lim, A metamaterial with sign-switching and discontinuous Poisson's ratio, International Journal of Solids and Structures 305, 113095 (2024)

[16] T.-C. Lim, Metamaterial with tunable positive to negative Poisson's ratio inspired by the Saint Andrew's Cross, Next Materials 9, 100954 (2025)

[17] K.E. Evans, M.A. Nkansah, I.J. Hutchinson, S.C. Rogers, Molecular network design, Nature 353, 124 (1991)

[18] L. Rothenburg, A.A. Berlin, R.J. Bathurst, Microstructure of isotropic materials with negative Poisson's ratio, Nature 354, 470-472 (1991)

[19] F. Nazare, A. Alderson, Models for the prediction of Poisson's ratio in the 'α-cristobalite' tetrahedral framework, Phys. Status Solidi (b) 252, 1465-1478 (2015)

[20] J.N. Grima, R. Gatt, A. Alderson, K.E. Evans, An alternative explanation for the negative Poisson's ratios in α-cristobalite, Mater. Sci. Eng. A 423, 219-224 (2006)

[21] Y.T. Yao, K.L. Alderson, A. Alderson, Modeling of negative Poisson's ratio (auxetic) crystalline cellulose I_β, Cellulose 23, 3429-3448 (2016)

[22] J.W. Narojczyk, K.V. Tretiakov, K.W. Wojciechowski, Poisson's ratio of f.c.c. hard-sphere crystals with cubic supercells containing four nanochannels filled by hard spheres of another diameter, Phys. Status Solidi (b) 259, 2200464 (2022)

[23] J.W. Narojczyk, K.W. Wojciechowski, J. Smardzewski, K.V. Tretiakov, Auxeticity tuning by nanolayer inclusion ordering in hard sphere crystals, Materials 17, 4564 (2024)

[24] R. Soutas-Little, *Elasticity*, Dover, New York, NY, USA, 1973.

[25] K.W. Wojciechowski, Constant thermodynamic tension Monte Carlo studies of elastic properties of a two-dimensional system of hard cyclic hexamers, Molecular Physics 61, 1247-1258 (1987)

[26] K.W. Wojciechowski, Two-dimensional isotropic system with a negative Poisson ratio, Physics Letters A 13, 60-64 (1989)
[27] K.W. Wojciechowski, Remarks on Poisson ratio beyond the limits of the elasticity theory, Journal of the Physical Society of Japan 72, 1819-1820 (2003)
[28] Y.C. Wang, M.W. Shen, S.M. Liao, Microstructural effects on the Poisson's ratio of star-shaped two-dimensional systems, Physica Status Solidi (b) 254, 1700024 (2017)
[29] Y.C. Wang, Negative Poisson's ratio in plane elasticity. In Encyclopedia of Continuum Mechanics, eds. H. Altenbach and A. Ochsner (Berlin: Springer). 1800-1806, 2019
[30] R.S. Lakes, Cubic Lattice Rib Shape: Tuning of Poisson's Ratio and Cosserat Characteristic Length, Phys. Status Solidi B, 2500330 (2025)
[31] R. Lakes, Anticlastic Curvature and Material Freedom, Phys. Status Solidi B, 2500039 (2025)
[32] D. Prall, R.S. Lakes, Properties of a chiral honeycomb with a Poisson's ratio -1, Int. J. Mech. Sci 39, 305-314 (1997)
[33] C.S. Ha, E. Hestekin, J. Li, M.E. Plesha, R.S. Lakes, Controllable thermal expansion of large magnitude in chiral negative Poisson's ratio lattices, Phys. Status Solidi (b) 252, 1431-1434 (2015)
[34] Y.C. Wang, T.W. Ko, X. Ren, Effective mechanical responses of a class of 2d chiral materials, Phys. Status Solidi (b) 257, 2000277 (2020)
[35] R.S. Lakes, B. Huey, K. Goyal, Extended Poisson's ratio range in chiral isotropic elastic materials, Phys. Status Solidi (b). 259, 2200336 (2022)
[36] R.S. Lakes, B. Huey, Poisson's ratio beyond the classically allowable range in chiral isotropic elastic materials: effect of k and experiment, Phys. Status Solidi (b) 261, 2300411 (2024)
[37] Y.C. Wang, T.C. Liao, K.W. Tan, SM Aizikovich, Bandgap properties of a class of chiral and achiral metamaterials, Sixty Shades of Generalized Continua, Springer, 693-704, 2023
[38] Y.C. Wang, T.W. Ko., K.W. Tan, Effective viscoelastic properties of chiral structures with hierarchy. In: Altenbach H., Eremeyev V.A., Galybin A., Vasiliev A. (eds) Advanced Materials Modelling for Mechanical, Medical and Biological Applications. Advanced Structured Materials, vol 155, pp. 429-440, Springer, Cham (2022)
[39] R.S. Lakes, T. Lee, A. Bersie, Y.C. Wang, Extreme damping in composite materials with negative-stiffness inclusions, Nature 410, 565-567 (2001)
[40] Y.C. Wang, R.S. Lakes, Extreme thermal expansion, piezoelectricity, and other coupled field properties in composites with a negative stiffness phase, Journal of Applied Physics 90, 6458-6465 (2001)
[41] R. Lakes, W. Drugan, Dramatically stiffer elastic composite materials due to a negative stiffness phase? Journal of the Mechanics and the Physics of Solids 50, 979-1009 (2002)
[42] Y.C. Wang, R.S. Lakes, Stable extremely-high-damping discrete viscoelastic systems due to negative stiffness elements, Applied Physics Letters 84(22), 4451-4453 (2004)
[43] Y.C. Wang, R.S. Lakes, Composites with inclusions of negative bulk modulus: extreme damping and negative Poisson's ratio, Journal of Composite Materials 39, 1645-1657 (2005)
[44] T. Jaglinski, D. Kochmann, D. Stone, R.S. Lakes, Composite materials with viscoelastic stiffness greater than diamond, Science 315, 620-622 (2007)
[45] Y.C. Wang, R.S. Lakes, Stability of negative stiffness viscoelastic systems, Quarterly of Applied Mathematics 63(1), 34-55 (2005)

[46] R. Lakes, K.W. Wojciechowski, Negative compressibility, negative Poisson's ratio, and stability, Physica Status Solidi (b) 245, 545-551 (2008)
[47] Y.C. Wang, C.C. Ko, Stability of viscoelastic continuum with negative-stiffness inclusions in low frequency range, Physica Status Solidi (b) 250, 2070-2079 (2013)
[48] Y.C. Wang, C.C., Ko, K.W. Chang, Anomalous effective viscoelastic, thermoelastic, dielectric and piezoelectric properties of negative-stiffness composites and their stability, Physica Status Solidi (b) 252, 1640-1655 (2015)
[49] Y.C. Wang, C.C. Ko, K.W. Chang, T.W. Ko, Negative-stiffness composite systems and their coupled-field properties, Continuum Mechanics and Thermodynamics 33, 1857-1872. doi:10.1007/s00161-021-01021-3 (2021)
[50] T. Hewagee, K. Alderson, A. Alderson, F. Scarpa, Double-negative mechanical metamaterials displaying simultaneous negative stiffness and negative Poisson's ratio properties, Advanced Materials 28, 10323-10332 (2016)
[51] R. Lakes, Cellular solid structures with unbounded thermal expansion, Journal of Materials Science Letters 15, 475-477 (1996)
[52] R. Lakes, Cellular solids with tunable positive or negative thermal expansion of unbounded magnitude, Applied Physics Letters 90, 221905 (2007)
[53] T.C. Lim, Anisotropic and negative thermal expansion behavior in a cellular microstructure, J. Mater. Sci. 40, 3275-3277 (2005)
[54] J.L. Cribb, Shrinkage and thermal expansion of a two phase material, Nature 220, 576-577 (1968)
[55] L. Cabras, M. Brun, D. Misseroni, Micro-structured medium with large isotropic negative thermal expansion, Proc. R. Soc. A 475, 20190468 (2019)
[56] J.N. Grima, E. Manicaro, D. Attard, Auxetic behaviour from connected different-sized squares and rectangles, Proceedings of the Royal Society A 467, 439-458 (2011)
[57] J.N. Grima, M. Bajada1, S. Scerri, D. Attard, K.K. Dudek, R. Gatt, Maximizing negative thermal expansion via rigid unimodes: a geometry-based approach, Proc. R. Soc. A 471, 20150188 (2015)
[58] K.K. Dudek, D. Attard, R. Caruana-Gauci, K.W. Wojciechowski, J.N. Grima, Unimode metamaterials exhibiting negative linear compressibility and negative thermal expansion, Smart Mater. Struct. 25, 025009 (2016)
[59] J.N. Grima, K.E. Evans, Auxetic behavior from rotating squares, Journal of Materials Science Letters 19, 1563-1565 (2000)
[60] J.N. Grima, P.-S. Farrugia, R. Gatt, V. Zammit, A system with adjustable positive or negative thermal expansion, Proc. R. Soc. A 463, 1585-96 (2007)
[61] G. Jefferson, T.A. Parthasarathy, R.J. Kerans, Tailorable thermal expansion hybrid structures, International Journal of Solids and Structures 46, 2372-2387 (2009)
[62] D. Li, J. Ma, L. Dong, R.S. Lakes, A bi-material structure with Poisson's ratio tunable from positive to negative via temperature control, Materials Letters 181, 285-288 (2016)
[63] T.C. Lim, Metacomposite with auxetic and in situ sign reversible thermal expansivity upon temperature fluctuation, Composites Communications 19, 30-36 (2020)
[64] T.-C. Lim, An anisotropic negative thermal expansion metamaterial with sign-toggling and sign-programmable Poisson's ratio, Oxford Open Materials Science 2, itac007 (2022)
[65] T.-C. Lim, An auxetic metamaterial with tunable positive to negative hygrothermal expansion by means of counter-rotating crosses, Phys. Status Solidi B 258, 2100137 (2021)

[66] M.T. Dove, H. Fang, Negative thermal expansion and associated anomalous physical properties: review of the lattice dynamics theoretical foundation, Rep. Prog. Phys. 79, 066503 (2016)
[67] Y. Ishibashi, M. Iwata, A microscopic model of a negative Poisson's ratio in some crystals, Journal of the Physical Society of Japan 69, 2702-2703 (2000)
[68] M.C. Rechtsman, F.H. Stillinger, S. Torquato, Negative thermal expansion in single component systems with isotropic interactions, J. Phys. Chem. A 111, 12816-12821 (2007)
[69] Y.C. Wang, K.W. Tan, T.W. Ko, T.C. Liao, Numerical study of simultaneously negative thermal expansion and Poisson's ratio in a class of auxetic structures, Physica Status Solidi (b) 259, 2200418 (2022)
[70] Y.C. Wang, Y. Sapsathiarn, T.C. Liao, Study of thermoelastic metamaterials simultaneously exhibiting negative thermal expansion and negative Poisson's ratio, The 14th TSME International Conference on Mechanical Engineering, Pattaya, Thailand, 10–13 December, 2024.
[71] A.A. Pozniak, J. Smardzewski, K.W. Wojciechowski, Computer simulations of auxetic foams in two dimensions, Smart Materials and Structures 22, 084009 (2013)
[72] R.D. Cook, D.S. Malkus, M.E. Plesha, R.J. Witt, *Concepts and Applications of Finite Element Analysis, 4th Ed*., John Wiley & Sons, Hoboken, NJ, USA, 2001.
[73] COMSOL (Nov. 2025). website. http://www.comsol.com
[74] O.B. Pedersen, Thermoelasticity and plasticity of composites-I. mean field theory, Acta Metall. 31, 1795-1808 (1983)
[75] B.W. Rosen, Z. Hashin, Effective thermal expansion coefficients and specific heats of composite materials, Int. J. Engng. Sci. 8, 157-173 (1970)
[76] R. Christensen, R. (1979). *Mechanics of Composite Materials*, Wiley, New York, NY, USA, 1979.
[77] J.-S. Chen, X. Zhang, T. Belytschko, An implicit gradient model by a reproducing kernel strain regularization in strain localization problems, Comput. Methods Appl. Mech. Engrg. 193, 2827-2844 (2004)

Figures and Figure Captions

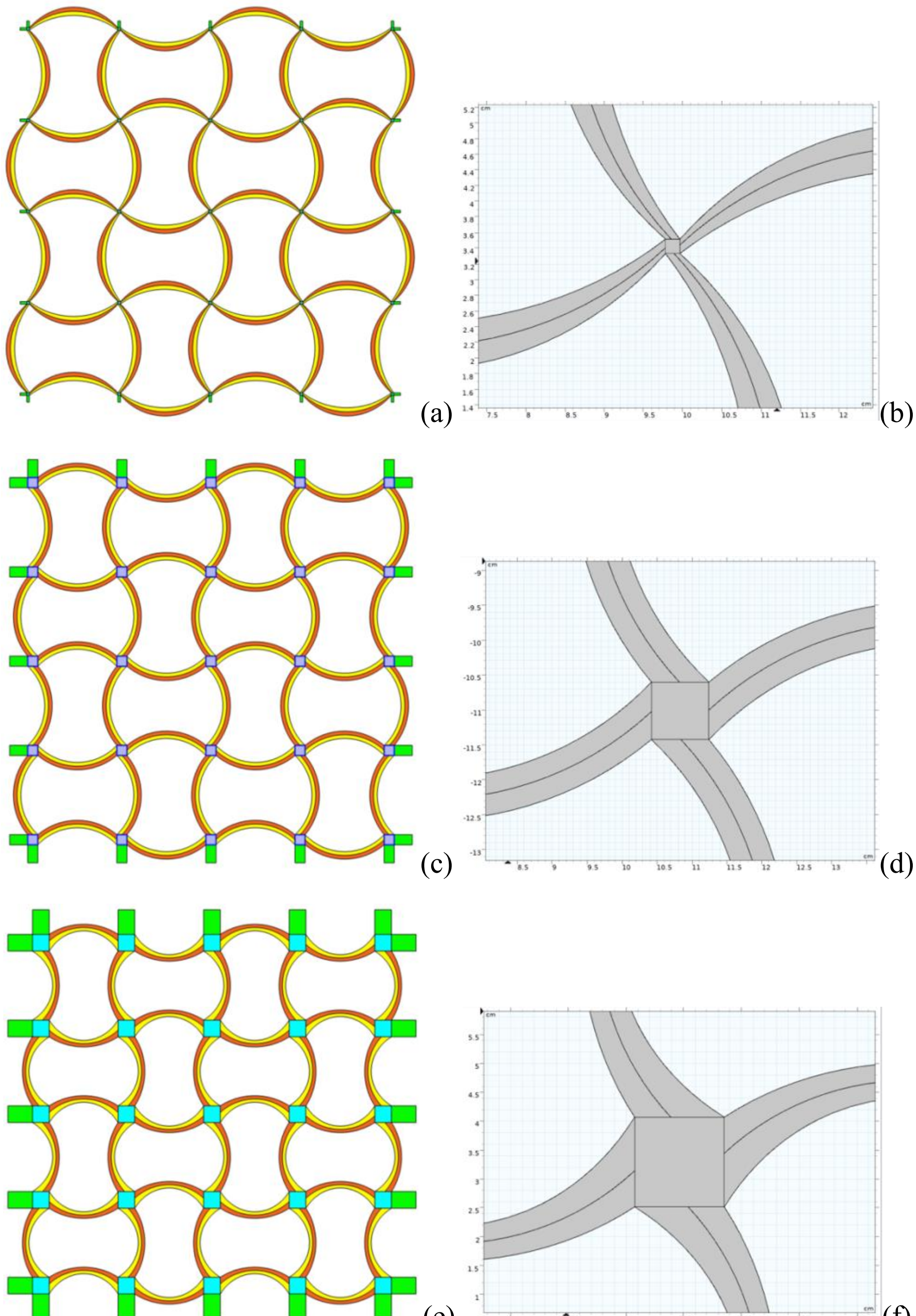

Figure 1. Auxetic structures with (a)(b) ‘small’, (c)(d) ‘medium’ and (e)(f) ‘large’ joints studied in this work.

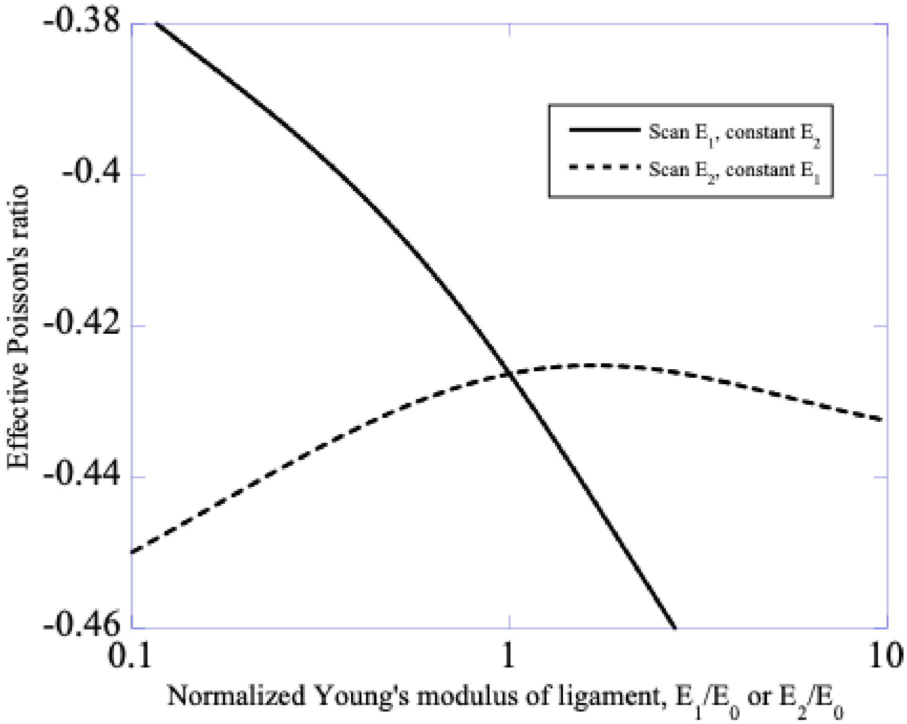

(a)

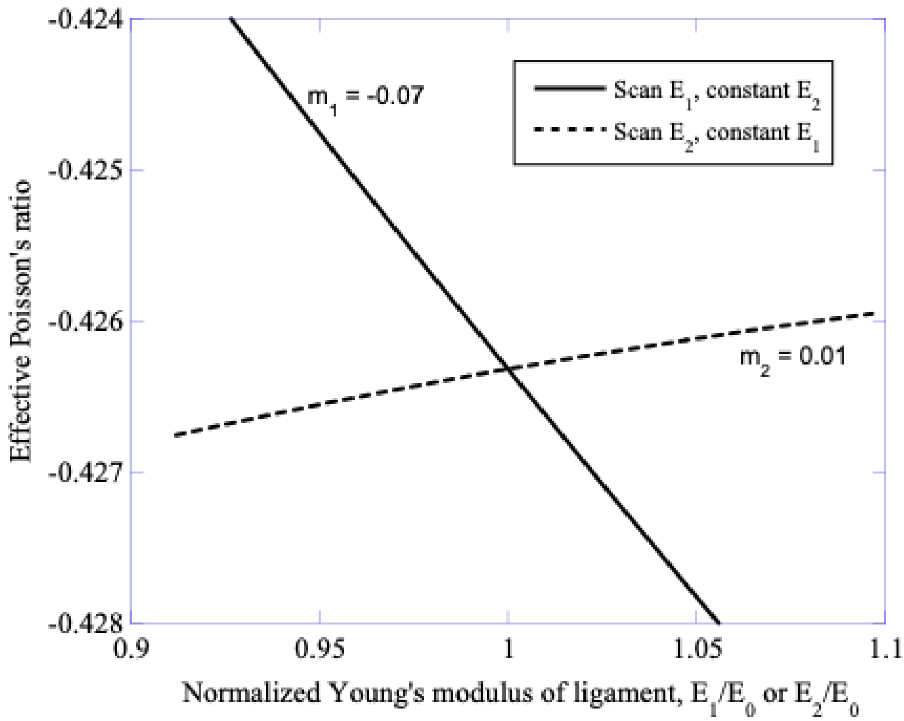

(b)

Figure 2. (a) Effective Poisson's ratio vs. Young's modulus of the bi-layered ligament, and (b) zoom-in of (a) near normalized Young's modulus of ligament equal to unity.

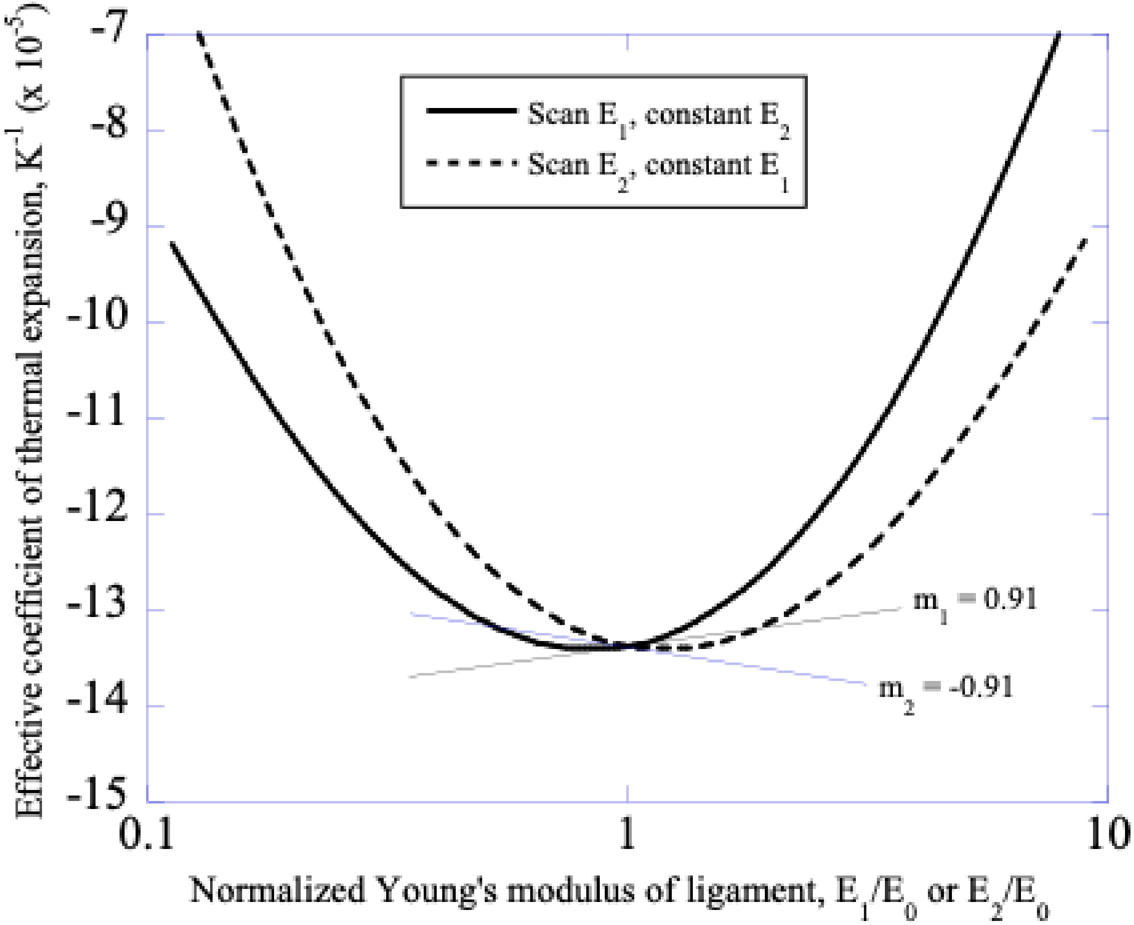

Figure 3. Effective coefficient of thermal expansion vs. the Young's modulus of the bi-layered ligament.

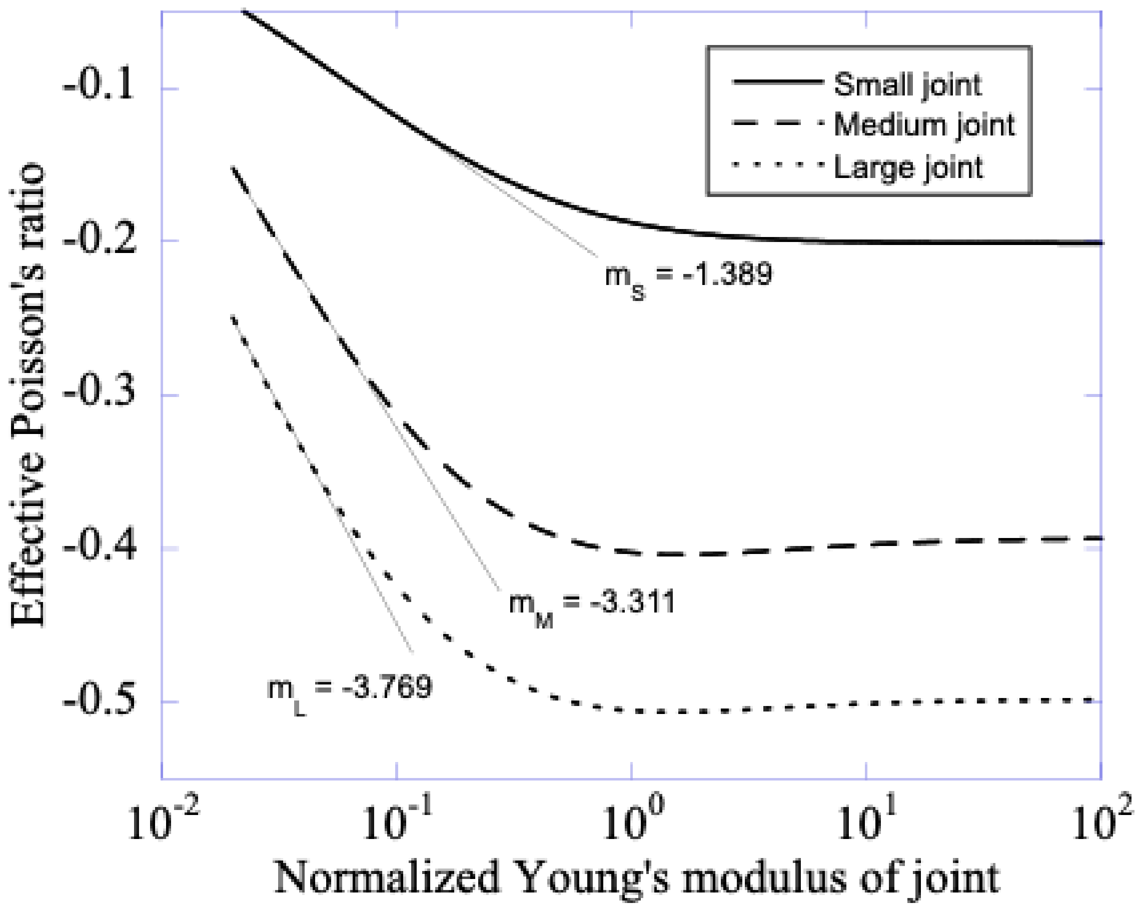

Figure 4. Effective Poisson's ratio vs. the normalized Young's modulus of the joints.

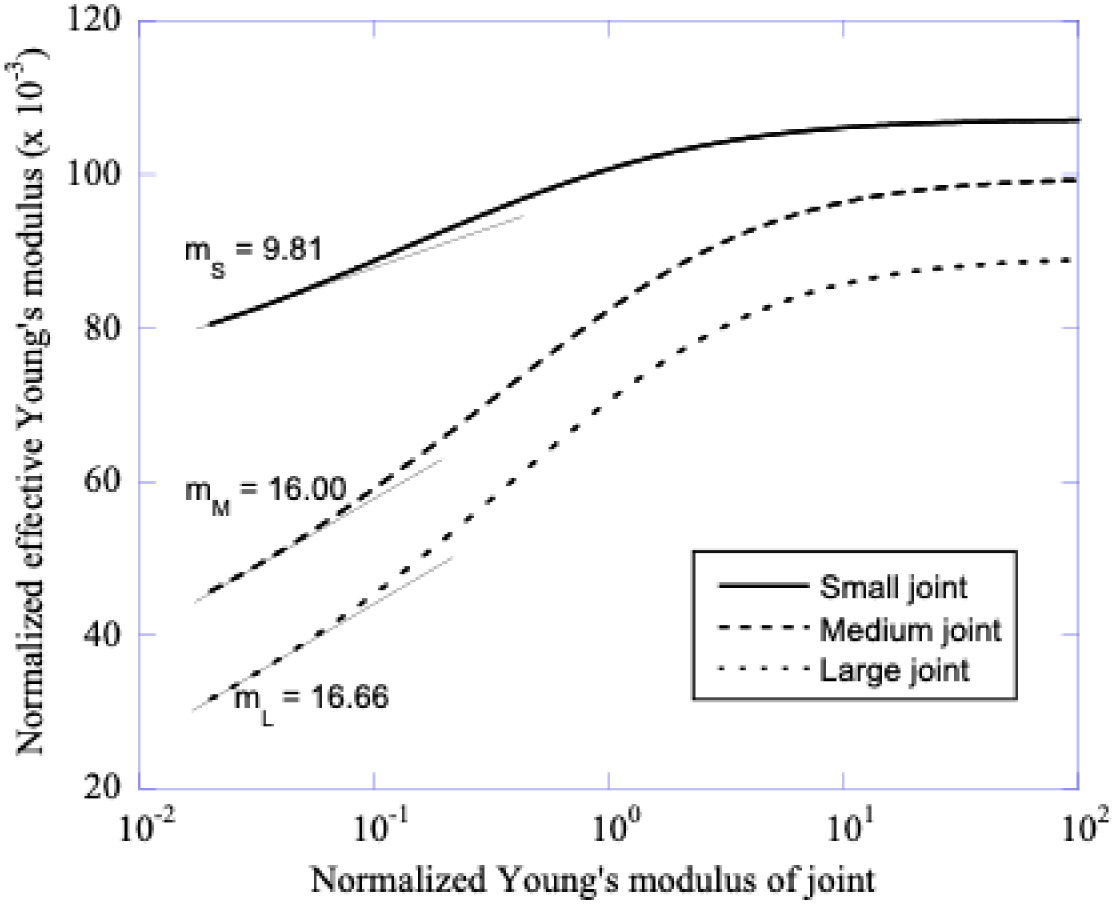

Figure 5. Normalized effective Young's modulus vs. the normalized Young's modulus of the joints.

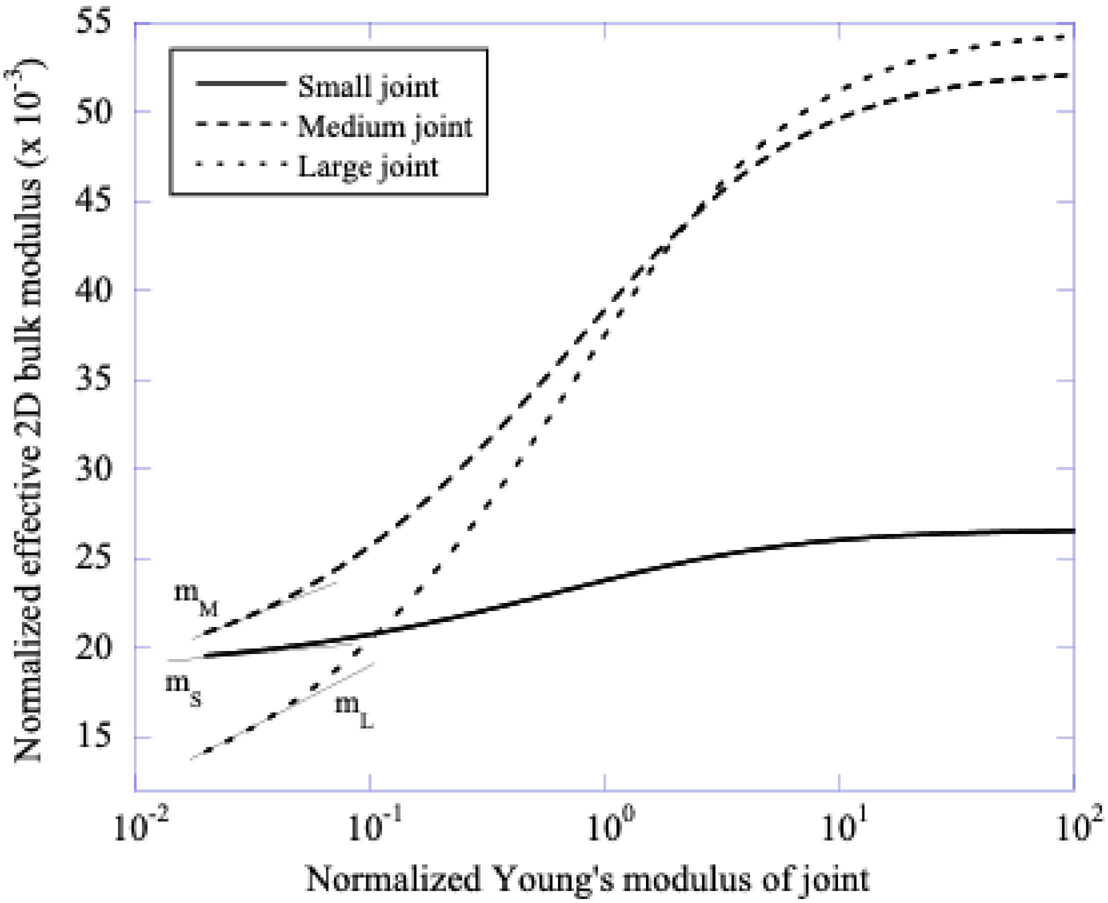

Figure 6. Normalized effective bulk modulus vs. the normalized Young's modulus of the joints. The asymptotic slopes near the left end are $m_S = 1.13$, $m_M = 4.60$, $m_L = 6.18$.

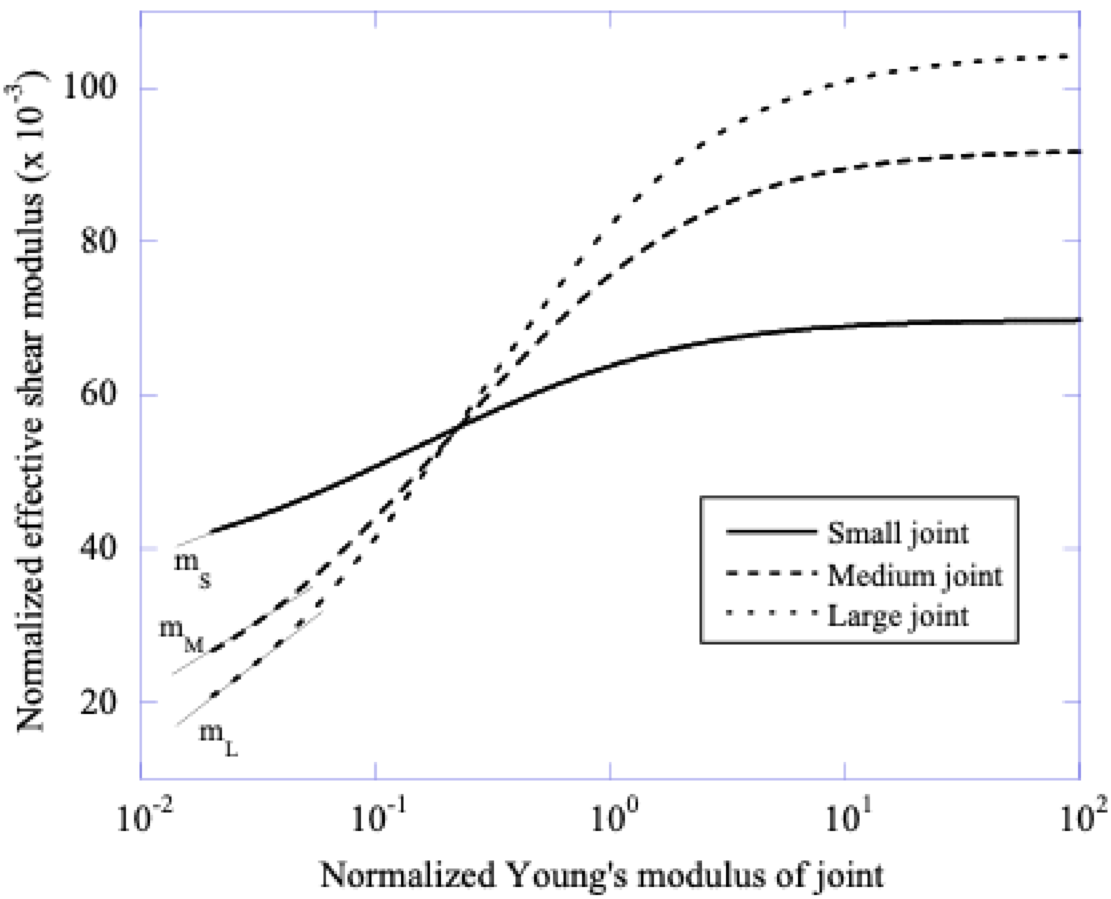

Figure 7. Normalized effective shear modulus vs. the normalized Young's modulus of the joints. The asymptotic slopes near the left end are $m_S = 10.00$, $m_M = 18.45$, $m_L = 21.68$.

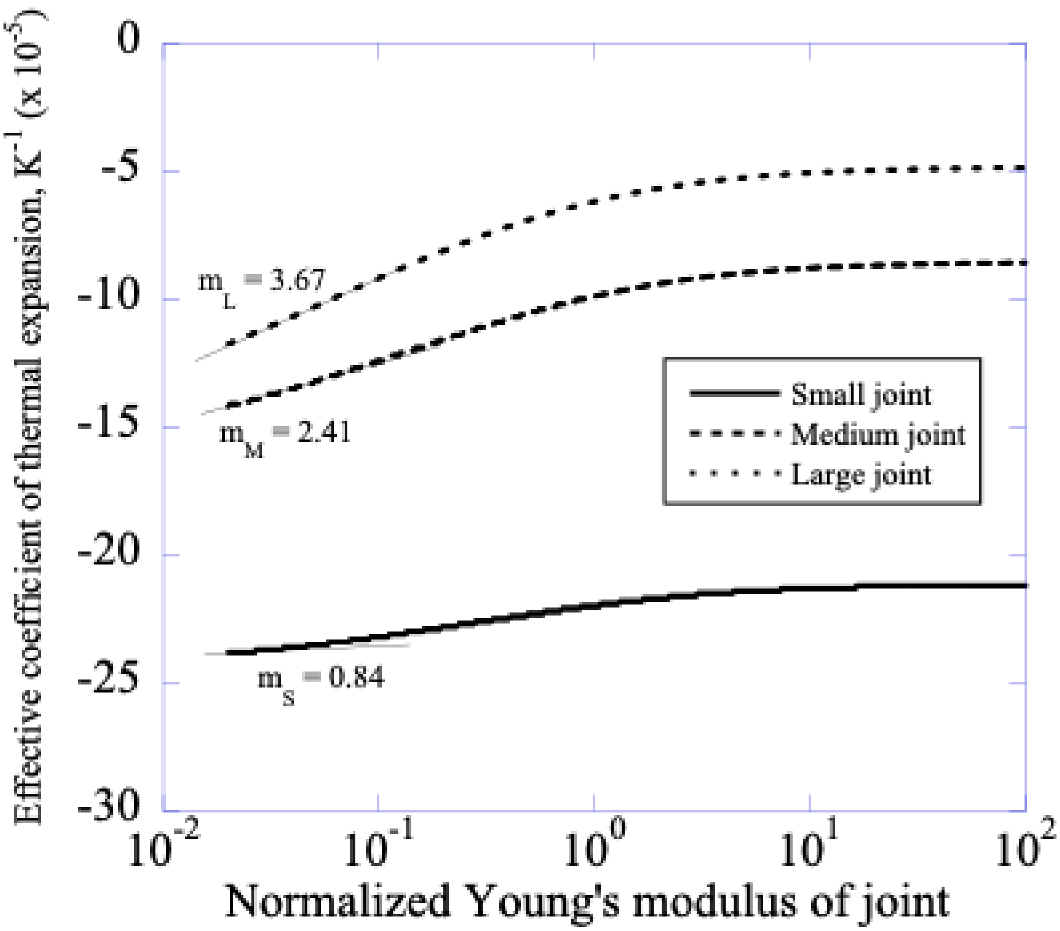

Figure 8. Effective coefficient of thermal expansion vs. the normalized Young's modulus of the joints. The asymptotic slopes near the left end are $m_S = 0.84$, $m_M = 2.41$, $m_L = 3.67$.

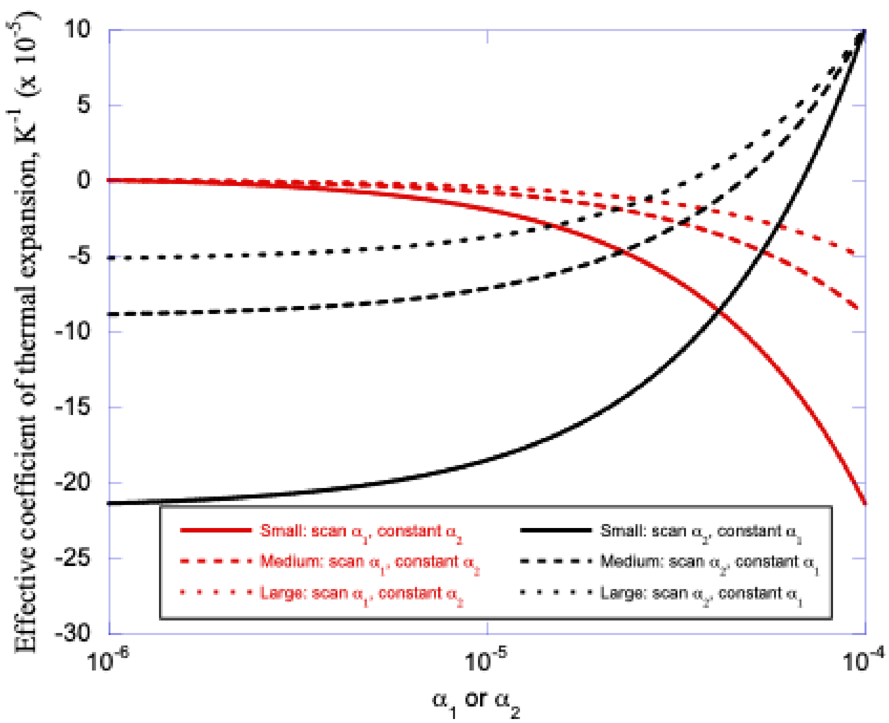

(a)

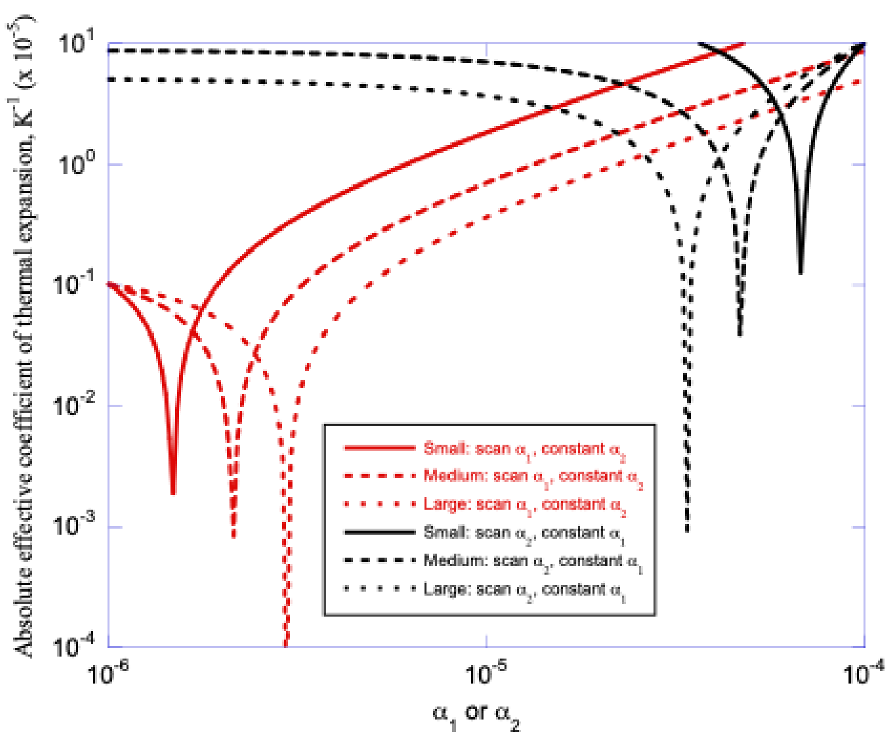

(b)

Figure 9. (a) Effective coefficient of thermal expansion vs. the bi-material's CTE α_1 or α_2., and (b) the absolute effective coefficient of thermal expansion vs. CTE.

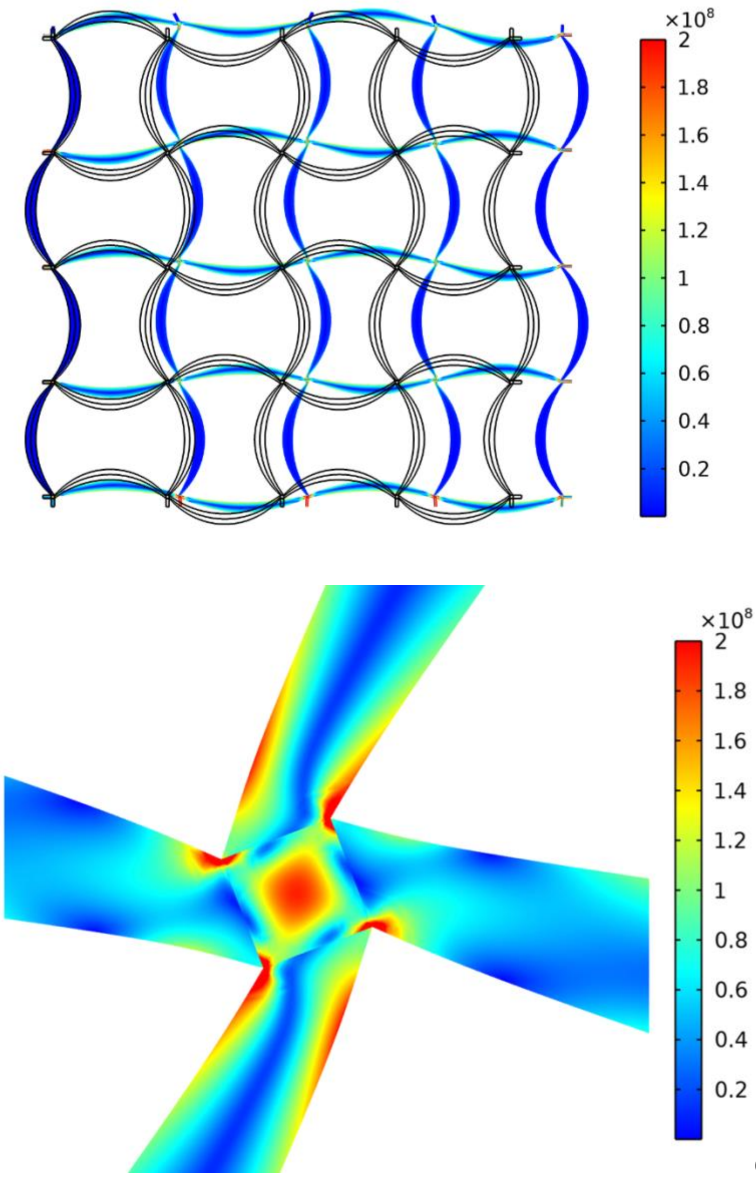

(a)

(b)

Figure 10. (a) Deformation of Figure 1 (a) under uniform temperature change, and (b) stress distribution around the 'small' joint. Color indicates the von Mises stress in units of Pa.